We are IntechOpen,
the world's leading publisher of
Open Access books
Built by scientists, for scientists

6,900
Open access books available

186,000
International authors and editors

200M
Downloads

154
Countries delivered to

Our authors are among the

TOP 1%
most cited scientists

12.2%
Contributors from top 500 universities

CLARIVATE ANALYTICS

BOOK CITATION INDEX

INDEXED

WEB OF SCIENCE™

Selection of our books indexed in the Book Citation Index
in Web of Science™ Core Collection (BKCI)

Interested in publishing with us?
Contact book.department@intechopen.com

Numbers displayed above are based on latest data collected.
For more information visit www.intechopen.com

Study on Multi-Phase Flow Field in Electrolysis Magnesium Industry

Ze Sun, Guimin Lu, Xingfu Song, Shuying Sun,
Yuzhu Sun, Jin Wang and Jianguo Yu
State Key Laboratory of Chemical Engineering
National Engineering Research Center for Integrated Utilization of Salt Lake Resources
East China University of Science and Technology, Shanghai
China

1. Introduction

Magnesium, the 8th most abundant element in the earth's crust, was discovered and isolated by Sir Humphrey in 1808. Magnesium is classified as an alkaline earth metal. It is found in Group 3 of the periodic table. It thus has a similar electronic structure to Be, Ca, Sr, Ba and Rd. The density of magnesium at 20°C is 1.738 g/cm³. At the melting point of 650°C this is reduced to 1.65 g/cm³. On melting there is an expansion in volume of 4.2%. Magnesium is the lightest metal in large-scale commercial use. After World War II, the magnesium industry attempted to develop magnesium for a number of applications. Most of its peacetime uses take advantage of the light weight or other chemical properties. The uses of magnesium as a structural material were, however, very few. The bulk was used as an alloying element in aluminium alloys. Other uses, such as deoxidation of steel, chemical and pyrotechnics, outweighed structural uses, especially in energy-saving and environmental protection applications was wide because of its contribution to reduce energy consumption and greenhouse gas emissions. The most successful peacetime application for magnesium was in the original German Volkswagen car that was designed by Ferdinand Porsche. The VW Beetle used large magnesium alloy die castings for the crankcase and the transmission housing (both cast in halves) plus a number of smaller castings. Each Beetle contained more than 20 kg of magnesium alloy. Many of the other applications developed during the World War II, could not be quickly converted to civilian uses. Some of the uses such as aircraft wheels and aircraft engine castings and troop carrying buses were modified and then used for the basis of civilian industries. With more attention to energy and environment, magnesium will hold greater promise as a new weight-saving replacement for denser steel and aluminum alloys, and demands for magnesium will increase sharply in the future. In recent decades, demands for magnesium and its productivity increased sharply shown in Figure 1, the world productivity of magnesium reached 860,000 tons at 2007.[1-3]

There are six sources of raw materials for the production of magnesium: magnesite, dolomite, bischofite, carnallite, serpentine and sea water. These sources differ in the magnesium content, in production methods, and in their origins. Some are mined from mines, some in open

mining, others originate in various processes carried out on sea water and salt lakes, and another material originates from the waste of the asbestos production process.
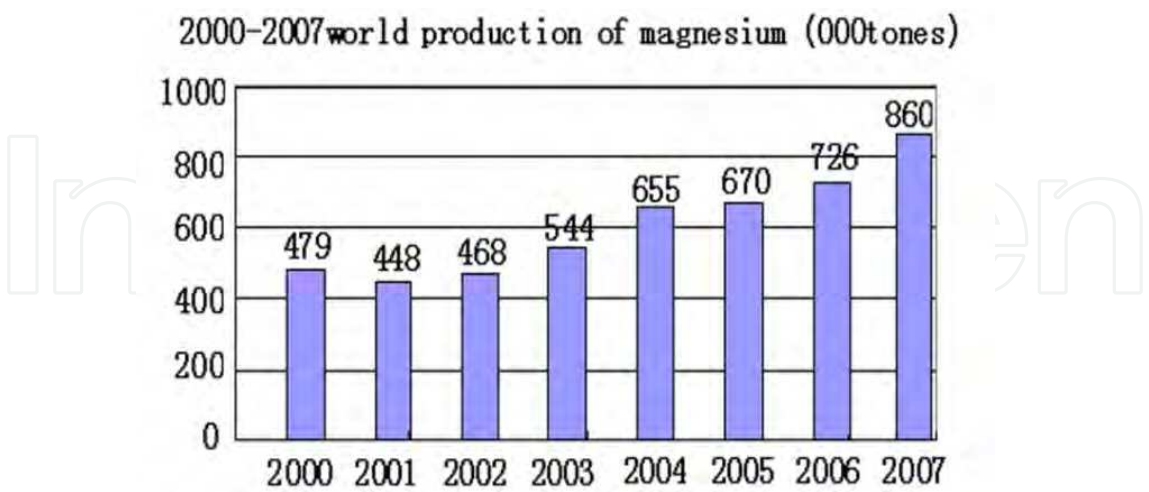

Fig. 1. 2000-2007 world production of magnesium

| Material	Chemical formula
Magnesite	$MgCO_3$
Dolomite	$MgCO_3 \cdot CaCO_3$
Bischofite	$MgCl_2 \cdot 6H_2O$
Carnallite	$MgCl_2 \cdot KCl \cdot 6H_2O$
Serpentine	$3MgO \cdot 2SiO_2 \cdot 6H_2O$
Sea water	$Mg^{2+}_{(aq)}$

Table 1. Raw materials and their molecular formula

1.1 Thermal reduction methods

The only ores used in the production of magnesium with thermal reduction technology are dolomite and magnesite. These ores are extracted through customary mining methods, mainly through open mining. The ore extracted from the mine undergoes calcination at temperatures of 700–1,000°C. At this temperature the material releases CO_2 gas, according to Eqs. (1) and (2), for magnesite and dolomite, respectively [3,4]:

$$MgCO_3 \rightarrow MgO_{(s)} + CO_{2(g)} \tag{1}$$

$$MgCO_3 \cdot CaCO_3 \rightarrow MgO \cdot CaO_{(s)} + 2CO_{2(g)} \tag{2}$$
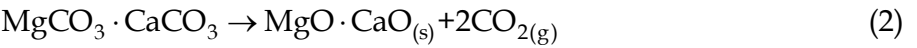
Following calcination the material is ground into a fine powder. Another main raw material that is used in thermal reduction is an alloy of silicon and iron called Ferrosilicon. The silicon content in this alloy is 65–85%, and at times the mix also contains small quantities of aluminum. The preparation of the ferrosilicon is carried out by reducing silica with coal, containing iron (scrap iron), at high temperatures [3,4]:

$$SiO_{2(s)}+2C_s+Fe \rightarrow Si(Fe)_{(s)}+2CO_{(g)} \tag{3}$$
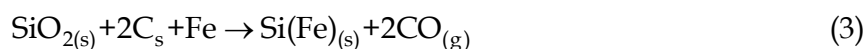
An additional material, which was used in the past as a thermal reduction agent, is Calcium carbide. The process of preparation of this material is relatively simple, but it requires high temperatures of about 1,800–2,000°C. Below is the reaction used in the production of this material:

$$CaO_{(s)}+3C_3 \rightarrow CaC_{2(s)}+CO_{(g)} \tag{4}$$

In China, most thermal reduction magnesium plants adopted the traditional Pidgeon process.

1.2 The pidgeon process[3,4]

This process was developed in the 1940s in Ontario Canada, by Prof. Pidgeon and the Timminco company. Lately, this process has received new attention and constitutes a central process in the magnesium production at a large number of Chinese manufacturers. The reaction that takes place is eqs. (5).

$$2MgO \cdot CaO_{(s)}+Si(Fe) \rightarrow 2Mg_{(s)}+Ca_2SiO_{4(1)} + Fe \tag{5}$$
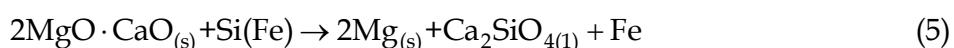
P=1 at′ ; T=1700℃ or P= 1mm Hg; T=1150-1200 ℃

A retort used in this process. The dimensions of the retort are 2.7–3.3 m with a diameter of 28–35 cm. The capacity of the retort is about 120 kg. The source of energy in the process carried out in China is normally coal, while the calcination process and the heating furnaces require 14–20 t of coal for the production of one ton of magnesium.

On completion of the process a magnesium crown is obtained, weighing 12–20 kg, which is then extracted from the upper part of the retort. Due to the usually high temperature, the magnesium in this case will contain high concentrations of aluminum, manganese, iron and other impurities. The above process can also be carried out with magnesite as an alternative to dolomite; the working conditions are almost identical and the reaction in this case is Eq. (6).

$$4MgO_{(s)}+Si(Fe) \rightarrow 2Mg_{(s)}+Mg_2SiO_{2(s)} + Fe \tag{6}$$

P= 10 mm Hg; T=1220 °C

Another version of the above process is carried out at a higher temperature, according to the reaction appearing in Eq. (7).

$$2MgO_{(s)}+Si(Fe)_{(s)} \rightarrow 2Mg_{(s)}+SiO_{2(1)} + Fe \tag{7}$$
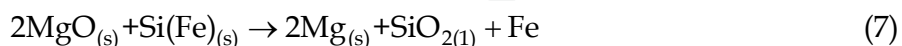
P=1 at′ ; T=2300℃ or P= 1mm Hg; T=1500 °C

The advantage of this reaction is the higher output from each retort (up to about 80%), while the disadvantages in this case are many. The main one being the higher temperature required for the process, 1,500 °C, about 300 °C higher than with the regular process. Work at a higher temperature usually causes the evaporation of impurities and a lower quality of material. In addition, there is accelerated amortization of tools, and this in addition to the higher cost of energy and the need for accessibility to magnesite.

1.3 Electrochemical method

The basic raw materials for the production of magnesium with the electrochemical process are generally divided into two: salts containing chloride and raw materials that must be transformed into salts containing chloride. Eventually, all the materials will become either bischofite or carnallite prior to drying and feeding into the electrolysis cells.

In the hydro magnesium process used in Canada the raw material for the process is magnesite, which is mined in mines (mainly in China). The magnesite is dissolved in a hot HCl solution, thus arriving at a magnesium chloride-rich solution:

$$MgCO_{3(s)} + 2HCl_{aq} \rightarrow MgCl_{2(aq)} + CO_{2(g)} \qquad (8)$$
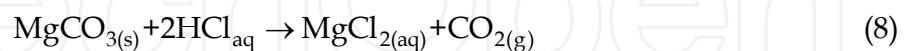
The acid solution must be hot for an efficient melting process. The basic ore of the magnesite is rich in various metallic impurities, sulfates and boron, which can be a problem at the electrolysis stage. Therefore, already at this stage a number of processes are carried out, whose purpose is to separate the impurities from the magnesium chloride.

1.4 Drying magnesium chloride salts

Carnallite, bischofite and their solutions contain large quantities of water. Carnallite and bischofite are hydrate salts containing six molecules of water per crystal and at times even additional water in attached form. The use of these materials in the electrolysis process requires the removal of all the water prior to the electrolysis.

Carnallite and bischofite tend to decompose in the hydrolysis reaction to magnesium oxide and HCl, at relatively low temperatures, and, therefore, the drying process is actually the most complicated and hardest stage in the electrolysis methods for the production of magnesium. In this matter it should be stated that most magnesium production R&D in the last decades has focused on the drying process for extraction of anhydrous magnesium chloride with low content of magnesium oxide.

Comparison with the thermal process, especially, the traditional Pidgeon process, the process of the magnesium production by electrolyzing the molten magnesium salt is more environmentally friendly. Moreover, in the electrolysis process, a high current efficiency (over 90%) can be reached with the application of the advanced diaphragmless electrolytic cell. Therefore, the research and development of the electrolysis technology of magnesium is more significant in future.

The electrolysis process of magnesium chloride is complicated, since there exit six important physical fields coupling with each other in the molten salt electrolyzer, namely electric field, magnetic field, flow field, temperature field, concentration field and stress field, all of which have the effects on the current efficiency, the direct current power consumption as well as the lifetime of the anode. Up to now, there are scarce researches on physical fields in the molten salt electrolyzer. So the optimization of the multi-fields is very significant for the optimum design of the large-scale magnesium electrolyzer. For example, in the electrolysis process of the molten magnesium salt, the current above 400kA, magnesium is produced from cathode as droplets, while the by-product chlorine gas is produced from anode as bubbles, both trying to rise the surface of the electrolyte as a result of the density difference with the electrolyte, so a three-phase flow under the strong electromagnetic field will be formed in the electrolytic cell[5,6]. During the electrolysis process, the multi-phase molten electrolyte circulation is very important to the current efficiency, better circulation better current efficiency in electrolysis magnesium industry. Many scientists and engineers have

paid attention to the flow field. Two measurements, cold model experiments and numerical simulation, are frequently adopted to study the flow field in electrolyzer. Holliday[7] used the similarity criteria to study electrolysis magnesium in low-density electrolytes. Burnakin used H_2O and argon gas to describe the hydrodynamics of a two-phase flow[8]. He controlled gas flow rate corresponding to current density from 0.1–0.4 A/cm^2 to simulate working electrolyzer. Brunakin also built equations for two-phase flow characteristics for a magnesium electrolyzer[9]. Korobov[10] and Shcherbinin[11-13] built mathematical model to simulate the temperature and electric fields in the magnesium electrolyzer. Agalakov[14] investigated the flow field of the multiphase flow in the electrolyzer by the computational numerical simulation with the two-dimensional mathematical model under the following assumptions and simplify.

- Only focused on the flow phenomena
- Two-dimensional model
- Steady flow
- Bubbles with uniform radius
- No interaction between bubbles
- Flow field without electromagnetic force

He got two circulations in electrolyzer, the main circulation was the transportation circulation and the small circulation would be resulted in the damage of the back wall. Author's previous work established mathematical model of flow field and validated the math model using particle image velocimetry (PIV) data[15]. Gökhan[16] used new style electrolyzer to produce magnesium, and studied the fluid characteristics in the electrolyzer.

2. Method of study flow field in electrolysis magnesium

2.1 Cold model

In building a cold model relative to the original system, some similarity criteria are as follows:

1. Geometric Similarity

    It is satisfied with Geometric Similarity requirements when the ratio of any length in model system to the corresponding length in the original system is the same everywhere.

2. Dynamic Similarity

    A physical model is thought to be dynamic similarity with the original model when the magnitude of forces that cause movement at corresponding location in each model is in a fixed ratio. How to choose dynamic similarity condition is the key to successfully simulate the flow characteristic in the original system.

3. Kinematic Similarity

    Kinematic similarity means similarity of motion. Velocity is kept in the close fixed ratio in the corresponding locations between the model system and original system.

4. Chemical Similarity

    Chemical similarity concerns the establishment of the necessary conditions in the model so that the rate of chemical reaction at any location is proportional to the rate of the same reaction at the corresponding time and location in the prototype.

During establishing a cold model, it is difficult to satisfy all the similarity criteria simultaneously. But it is necessary to comply with important criteria that include some significant variables and try to follow the other similarity criteria.

According to the similarity criteria, such as geometric similarity, dynamic similarity, kinematic similarity, cold models of magnesium electrolysis cell were built[15].

A laboratory scale cold model experiment was set up. A transparent vessel had the shape of a cube with 104×4×10 cm in dimension. Lead anodes and graphite cathodes with 6×2×0.2 cm were installed in parallel with each other, as shown as in Figure 2. The distance between anode and cathode was 80 mm. The electrolyte was zinc sulfate solution with 2 mol/L concentration. Direct current was added to anode and cathode with various current densities. In electrolyzing, zinc was deposited on cathodes and oxygen was released from anodes and moves upward the surface of the electrolyte.

The Particle Image Velocimetry system (PIV) is provided by Dantec Dynamics. It is a specifically novel non-intrusive visualization experimental technique, set up to provide instantaneous velocity vector measurements in a cross-section of the model. The available camera is part of the PIV system from Dantech Dynamics. Cameras use high-performance progressive-scan-interline CCD chips which includes 1018 ×1008 light-sensitive cells and an equal number of storage cells.

The target area was in the middle of the electrolytic cell perpendicular to the surface of electrode and limited one pair of electrodes. The area was located the mirror plane on electrodes. Usually, seeding particles are added to the water in order to observe the motion of the transparent water. In our experimental system, oxygen bubbles generated on anodes are small enough as tracking particles. The FlowMap software was used for post processing the images.

(a) cold model   (b)PIV

Fig. 2. Cold model experiment and PIV instrument

Figure 3 shows the typical streamlines of the flow field at a cross-section perpendicular to electrodes in cold model experiment system, measured by PIV instrument. In Figure 3, anode was at the left side of the picture, and the opposite side was cathode. The high density of streamlines represents the high flow velocity. A bigger eddy was formed nearby anode, mainly as a result of the upward movement of oxygen bubbles released from anode at electrolyzing. This phenomenon is explained as pumping effects on the flow field, that is, with oxygen bubbles leave to the surface of electrolyte, the space which had been occupied by oxygen bubbles became empty, and the nearby electrolyte would fill into the space under the fluid pressure.
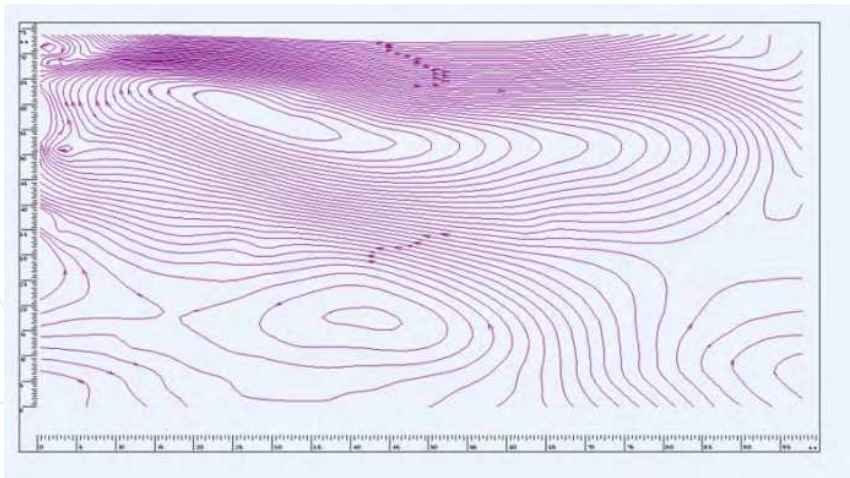
Fig. 3. Streamlines of the flow field in cold model experiment with 0.35 A/cm² current density measured by PIV (anode: left, cathode: right)

The flow velocity distribution between anode and cathode was measured by PIV instrument, shown in Figure 4. The target position was at 10% height of anode near the electrolyte surface. The flow velocities increase along the distance from both anode and cathode, respectively, and reach the maximal flow velocity in the middle of one pair of electrodes. Because of the oxygen bubbles continuously upward movement on anode, the position corresponding to the maximal flow velocity was slight close to cathode.
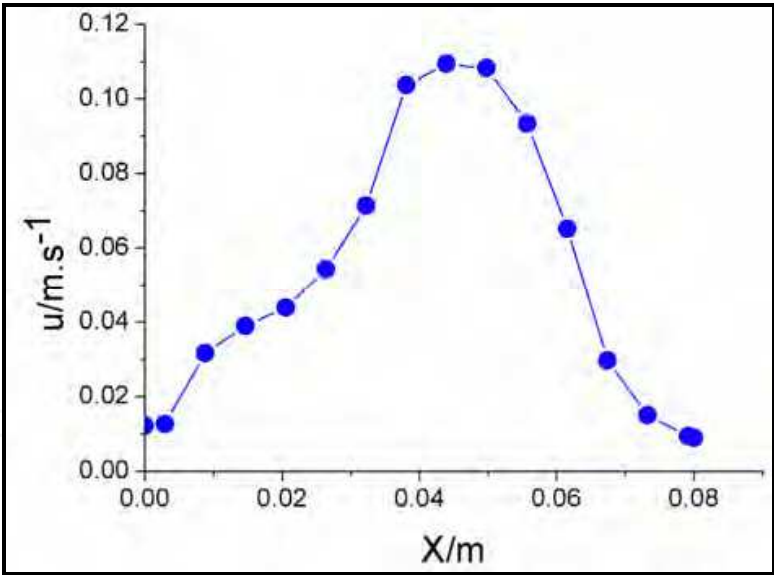

Fig. 4. Flow velocity distribution between experiment at 0.35A/cm² current density. (anode:left, cathode: right)

2.2 Cold model 2
According to geometric similarity, systems are considered to be geometrically similar when the ratio of any length in one system to the corresponding length in the model system is the same everywhere.
In the experiment, the physical model is built according to 1:5 ratio to an original model, as shown in Table 2.

Parameters	Cell parameters for the plant (mm)			Parameter for the physical model (mm)		
whole size	X=6165	Y= 1870	Z=2065	X=420	Y= 374	Z=415
anode size	X=150	Y=1000	Z=2020	X=30	Y=200	Z=404
cathode size	X=50	Y=1000	Z=950	X=10	Y=200	Z=190
total cathode number	18			2		
total anode number	16			1		

Table 2. Size comparison between the cell and physical model

A physical model is thought to be dynamic similarity with the original model when the magnitude of forces that cause movement at corresponding location in each model is in a fixed ratio. How to choose dynamic similarity condition is the key to successfully simulate the flow characteristic in the electrolytic magnesium. For aluminum electrolysis cell, both the density differential ratio$((\rho_1-\rho_2)/(\rho_1+\rho_2))$ and dynamic interface tension$(T/(\rho_1+\rho_2))$[17] were used as dynamic similarity conditions to simulate the aluminum flow characteristic. The modeling phases were chosen according to dynamic similarity conditions of close dynamic surface tension, close density differential ratio and the close kinematic viscosity to simulate the flow characteristic in electrolytic magnesium, the details are shown in Table 3.

Model Parameters	Electrolysis cell (700°C)			Physical model cell (20°C)		
	Mg (liquid)	electrolyte	chloride	Silicon oil	water	Chloride
density (g/cm^3)	1.58	1.7	0.000903	0.927	0.998	0.00016
dynamic viscosity (cst)	0. 715	1	34	0.715	1	0.133
surface tension (mN/m)	0.547	108	—	0.022	72.88	—
dynamic surface tension $T/(\rho_1+\rho_2)$	32.9		—	37.76		—
density differential ratio $(\rho_1-\rho_2)/(\rho_1+\rho_2)$	0.0366		—	0.0368		—

Table 3. Comparison between the cell and physical model

Kinematic similarity means that velocity is kept in the close fixed ratio in the corresponding locations between the physical model system and original electrolytic magnesium. In this cold model, argon gas velocity is kept close to the molar flow rate of chlorine released in anode at anodic current density of 0.314 A/cm^3. The initial gas velocity in the physical model can be figured out according to the following formula.

$$V_{\text{gas}} = \frac{0.286 \times [80 + 48 \times (29.5 - D)] \times 60}{2 \times 96500} \tag{9}$$

D: distance between anode and the cell bottom; $[80+48\times(295-\mathrm{D})]$: total area of the immersed anode; 96500: electrochemical equivalent

In the electrolytic magnesium system, the relationship between magnesium collection rates and electrolyser structure has not figured out quantitatively because of the quite complicated flow characteristic. The effects of multi-parameters such as anode-cathode distance (ACD), the gradient angle for silicon oil leading channel (θ), depths of electrode (D), width of the service area (W), on recovery rate of magnesium(φ) are very significant. The cold model 2 was shown in fig. 5.

Split the anode into 10 chamber, drill the surface of each chamber with the small hole (Φ 0.5 mm), then the gas can release from the anode equable. As the gas, oil also release equable from the small hole in the cathode surface.

After a series of regression experiment in the physical modeling, the results were obtained as follows: ACD: anode-cathode distance; θ: the gradient angle for silicon oil leading channel; D: depths of electrode; W: width of the service area; Φ: recovery rate of oil
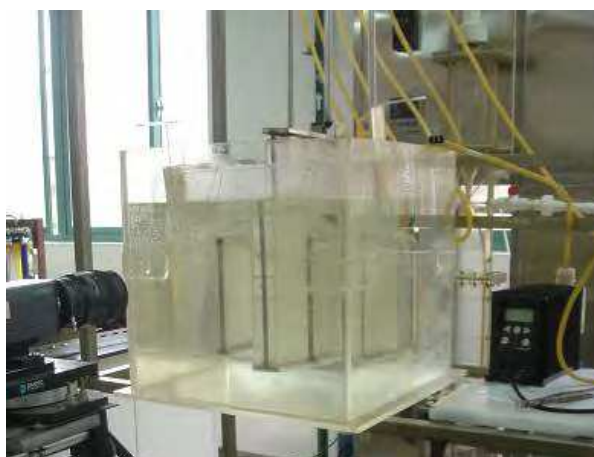

Fig. 5. Cold model of magnesium electrolyzer using silicon oil and argon

By variance analysis, the significance for the recovery rate of silicon oil is in the sequence of θ, ACD and D, and finally W. The recovery rate of silicon can reach the highest under the experimental conditions of 60 mm(ACD), 28 mm(D), 127 mm(W), 12°(θ) according to the experimental data processing.

The relationship between magnesium collection rates and electrolyser structure can be described by the following function formula. In this section , for the very first time we carried out physical model experiments and try to find out the relationship on the magnesium recovery and above variations, and build an quantitative formula between them, the equation as follows:

$$\Phi = -75.6 + 1.42(\text{ACD}) - 0.051D + 1.385W - 0.37\theta + 0.006(\text{ACD}) \times$$
$$D - 0.017(\text{ACD}) \times \theta - 0.003D \times W + 0.028W \times \theta - 0.013(\text{ACD})^2 - 0.007W^2 - 0.1\theta^2 \tag{10}$$

The single parameter experiment was carried out near the best experimental conditions to check the effect of each parameter on the recovery rate of silicon.

No.	ACD	D	W	θ	$\varPhi$
1	80	75	120	12	84
2	80	75	80	4	73.5
3	80	35	120	4	68
4	80	35	80	12	78.8
5	40	75	120	4	64.55
6	40	75	80	12	79.7
7	40	35	120	12	84.3
8	40	35	80	4	67.5
9	87.06	55	100	8	80.3
10	27.94	55	100	8	71.6
11	60	82.06	100	8	80.1
12	60	27.94	100	8	89.5
13	60	55	127.06	8	79
14	60	55	72.94	8	80.9
15	60	55	100	13.4	89
16	60	55	100	2.6	75.5
17	60	55	100	8	83.5

Table 4. Regression experiment and result
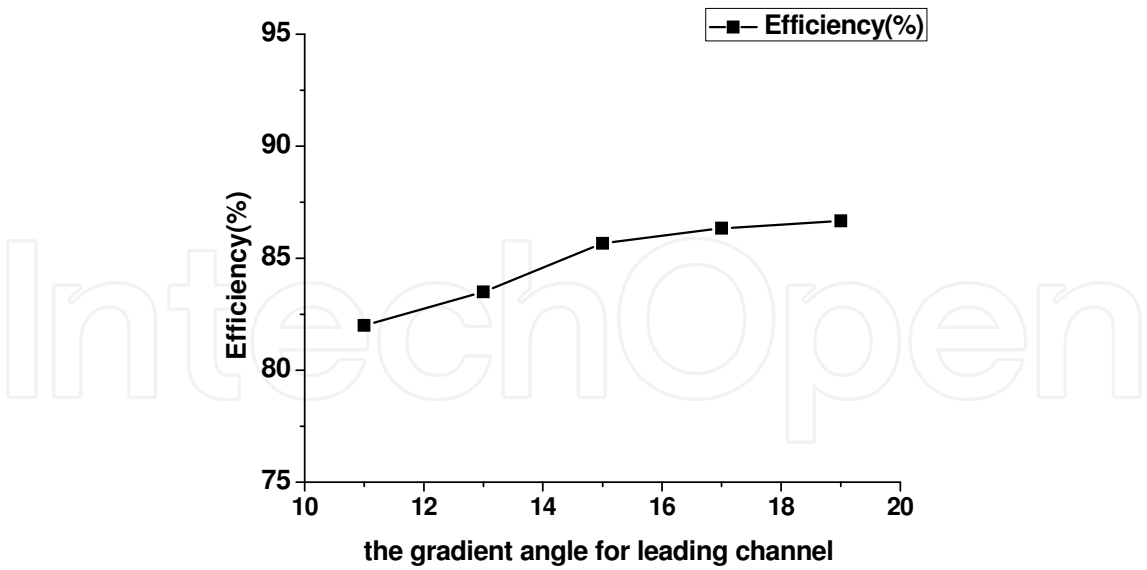
Fig. 6. The relationship between θ and φ

Fig. 6 showed the effects of the gradient angle for silicon oil leading channel (θ) on the recovery rate of oil. The recovery rate of silicon increase simultaneously with the increase of the gradient angle for silicon oil leading channel, and (φ) reach the highest recovery rate at (θ) of 12° and then maintained no change with increase of (θ).
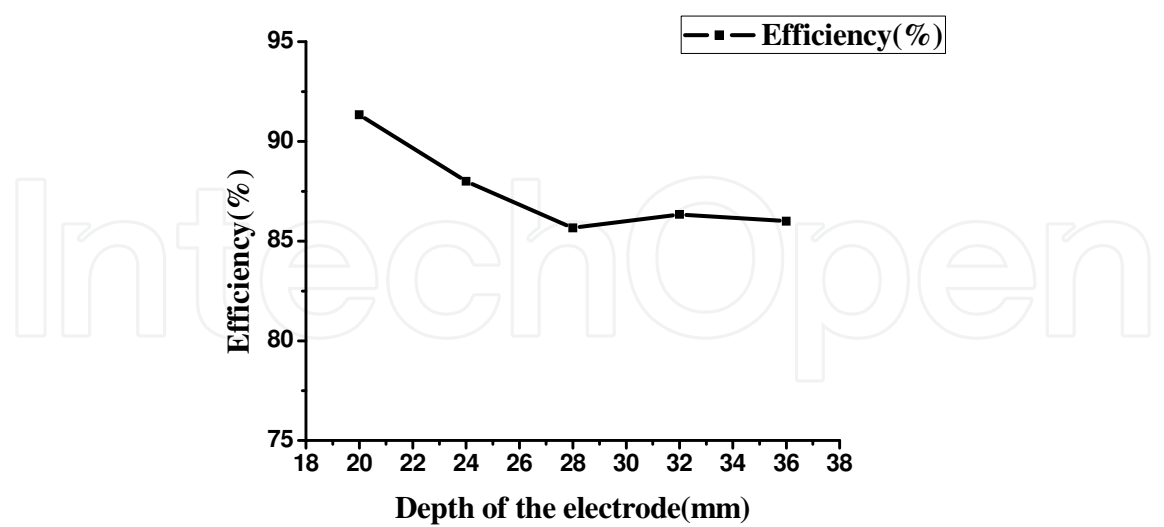
Fig. 7. The relation between *D* and *φ*

Fig. 7 gave the effects of depths of electrode (D) on recovery rate of silicon oil φ. It can be seen that the recovery rate increases with the increase of depth of electrode, and reaches the highest recovery rate of silicon oil at depth of electrode as 28mm. the largest recycle rate of silicon oil is 91.34 wt-% under the experimental conditions of 60 mm (ACD), 20 mm (D), 127 mm (W), 12° (θ). When the anode immerses in the electrolyte more deeply, more gas will releases into the electrolyte, which will cause the strong electrolyte circulation in the cell and more oil will be bring into the service area, therefore the recovery rate of silicon oil will be improved.
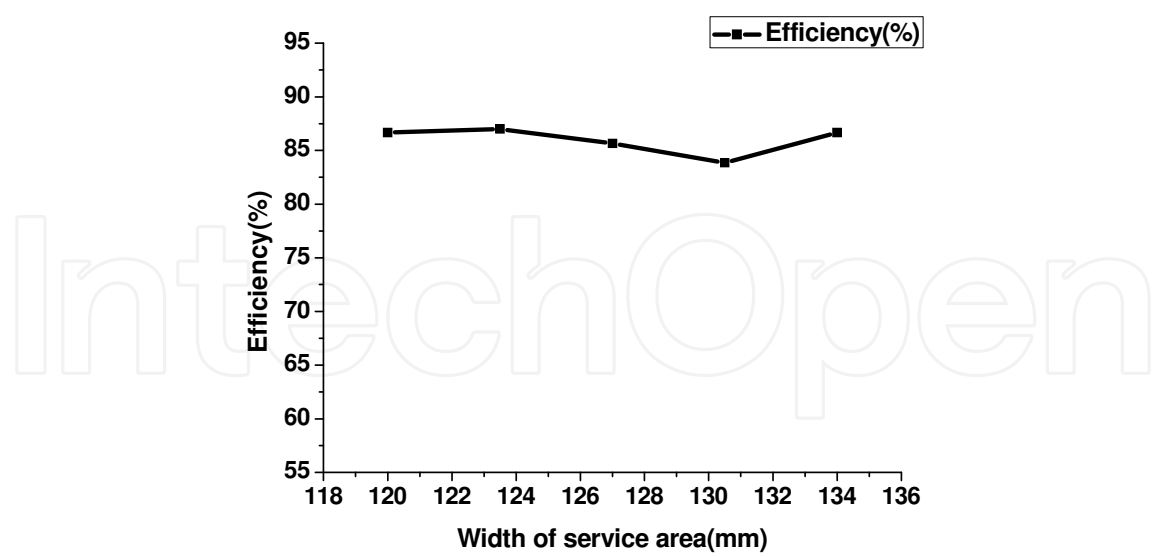
Fig. 8. The relation between *W* and *φ*

According to Fig. 8, near the best experiment conditions, the recovery rate of silicon was nearly the same. Fig. 9 displays the relationship between ACD and φ, as the W, near the best experiment conditions, in which the ACD is 6 cm, φ tent to be unrelated to ACD.
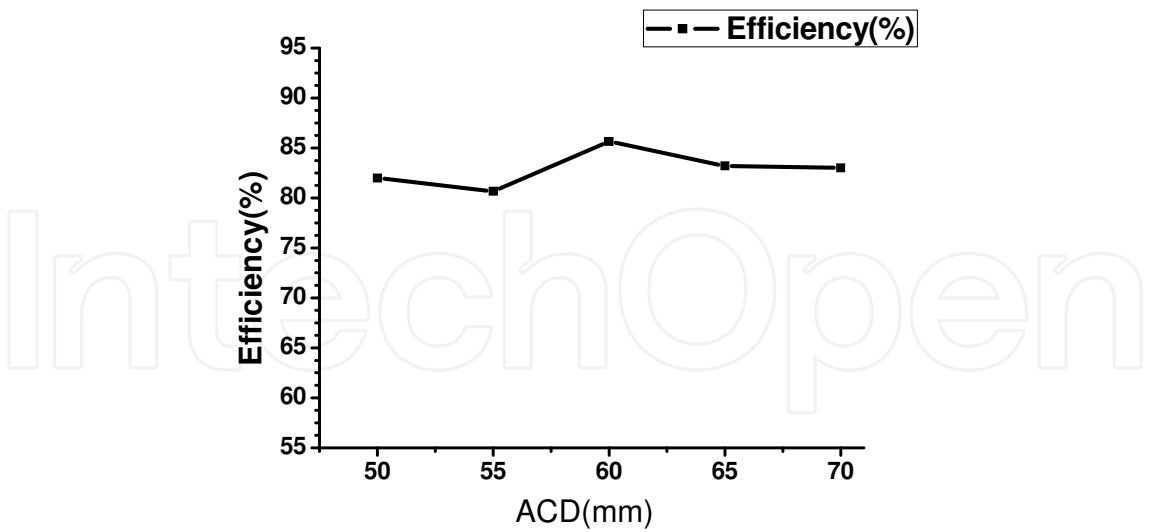
Fig. 9. The relation between ACD and φ

The effects of anodic shape on gas movement along the anode surface was investigated by the PIV, The spray angle for gas from anodic bottom to top maintains at 9° , and does not change with anodic shape and flow rate. The results were shown in fig. 10 and table 5.
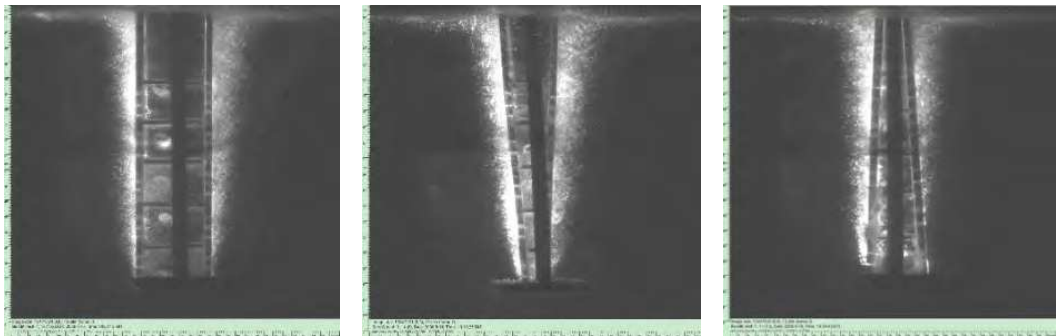

Fig. 10. Spray angle for rectangle, positive and negative dovetail anode

flow rate \ shape	rectangle anode	positive dovetail anode	negative dovetail anode
5 L/min	8.6°	8.8°	8.5°
10 L/min	9°	9°	8.7°
15 L/min	9°	9°	9.2°

Table 5. Value of the spray angle

3. Simulation method

Numerical simulation of three-phase flow field in magnesium electrolyzer involves several subjects including electromagnetism and fluid dynamics. The model leans on the following basic hypotheses[18]:

1. The electromagnetic fields satisfy the stationary Maxwell's equations, and Ohm's law is moreover supposed to be valid in the electrolyzer.
2. The fluids are immiscible, incompressible and Newtonian.
3. The chlorine gas is as another continuous phase.
    The electrical conductivity γ and magnetic permeability λ are constant, respectively.
4. Fluid without chemical reactions.

Electromagnetism is based on Maxwell equations and Ohm's law. The differential form of Maxwell partial differential equations is given as follows:

$$\nabla \times H = J + \frac{\partial D}{\partial t} \tag{11}$$

$$\nabla \times E = -\frac{\partial B}{\partial t} \tag{12}$$

$$\nabla \cdot D = \phi \tag{13}$$

$$\nabla \cdot B = 0 \tag{14}$$

Where H is the magnetic intensity vector, J is the conduction current density, D is the electric displacement vector, E is the electric field intensity vector, B is the magnetic flux density vector and ϕ is the free charge volume density.

The electromagnetic constitutive equations of simple isotropic material mediums can be expressed as:

$$D = \beta E \tag{15}$$

$$B = \lambda H \tag{16}$$

$$J = \gamma E \tag{17}$$

Where $\beta = \beta_r \beta_0$ is the absolute electric constant, $\lambda = \lambda_r \lambda_0$ is the absolute permeability and γ is the electric conductivity.

Fluid dynamics is based Navier–Stokes equations, for multi-phase, volume of fluid (VOF) was an effective method for three-phase flow in magnesium electrolyzer[12]. For the qth phase, the equations have the following forms:

Continuity equation

$$\frac{1}{\rho_q}\left[\frac{\partial}{\partial t}\left(\alpha_q \rho_q\right) + \nabla \cdot \left(\alpha_q \rho_q \vec{v}_q\right) = S_{\alpha q} + \sum_{p=1}^{n}\left(\overset{\bullet}{m}_{pq} - \overset{\bullet}{m}_{qp}\right)\right] \tag{18}$$

Where α_q was the volume fraction of qth phase in discrete volume; ρ_q was the density of qth phase; m_{pq} and m_{qp} were mass exchange between q^{th} phase and p^{th} phase, in the electrolyzer, the mass exchange was zero; $S_{\alpha q}$ was the source term, $S_{\alpha q} = 0$.

The volume fraction equation will not be solved for the primary phase; the primary-phase volume fraction will be computed based on the following constraint:

$$\sum_{q=1}^{n} \alpha_q = 1 \tag{19}$$

Considering the effects of electromagnetic field on molten salt, the Lorentz force was as source term in momentum equation:

$$\frac{\partial}{\partial t}\left(\rho \vec{v}\right) + \nabla \cdot \left(\rho \vec{v} \vec{v}\right) = -\nabla_p + \nabla \cdot \left[\mu\left(\nabla \vec{v} + \nabla \vec{v}^T\right)\right] + \rho \vec{g} + \vec{F} \tag{20}$$

Where F is the Lorentz force, and $F = J \times B$.

A single momentum equation is solved throughout the domain, and the resulting velocity field is shared among the phases. In order to get the solution of Navier–Stokes equations, turbulence model is essential to close set of equations. Turbulence model divides three types: direct numerical simulation (DNS), large eddy simulation (LES) and Reynolds-Averaged Navier-Stokes (RANS) Models. The most used model among the turbulence models is the Reynolds-Averaged Navier-Stokes (RANS) Models. The k-ε model is the most suitable one. In the case of the k-ε model, two transport equations are considered; one for the computation of the turbulent kinetic energy and one for the turbulent dissipation rate.

$$\frac{\partial}{\partial t}(\rho k) + \frac{\partial}{\partial x_j}(\rho u_j k) = \frac{\partial}{\partial x_j}\left[\left(\frac{\mu_t}{\sigma_{k0}}\right)\frac{\partial k}{\partial x_j}\right] + G_k - \rho\varepsilon \tag{21}$$

$$\frac{\partial}{\partial t}(\rho\varepsilon) + \frac{\partial}{\partial x_j}(\rho u_j \varepsilon) = \frac{\partial}{\partial x_j}\left[\left(\frac{\mu_t}{\sigma_{\varepsilon0}}\right)\frac{\partial \varepsilon}{\partial x_j}\right] + \frac{\varepsilon}{k}(C_{\varepsilon1}G_k - C_{\varepsilon2}\rho\varepsilon) \tag{22}$$

Where $G_k = \mu_t \frac{\partial u_i}{\partial x_j}(\frac{\partial u_j}{\partial x_i} + \frac{\partial u_i}{\partial x_j})$, C_μ, $C_{\varepsilon1}$, $C_{\varepsilon2}$, $\sigma_{\varepsilon0}$, σ_{k0} are constants, They are C_μ =0.09, $C_{\varepsilon1}$ =1.44, $C_{\varepsilon2}$ =1.92, $\sigma_{\varepsilon0}$ =1.3, σ_{k0} =1.0 respectively.

The solution of electromagnetic field can be made by using magnetic vector potential (MVP) method in ANSYS 11.0. The finite elements type SOLID 69 is used to get electric field and SOLID97 to get electromagnetic field. The flow field distribution is obtained by using Fluent 6.3. To solve the governing partial differential equations, Navier–Stokes equations, for the conservation of mass, momentum, and scalars such as turbulence in integral form, a control-volume technique and SIMPLE procedure are used. The momentum source term, Lorentz forces, is read by user defined function (UDF). All simulations are performed on a personal computer equipped with two processors, Intel core 6300 and 2 GB main memory running under the Windows operating system.

In the whole calculation process, coupled fields calculation is the main characteristic. Firstly, in order to get the electromagnetic field distribution, coupling calculation of electric field and electromagnetic field are undertaken, where electric field is as electromagnetic field's input. Secondly, considering effects of electromagnetic field during flow field calculation, flow field coupled electromagnetic field through taking Lorentz forces as source term in momentum equation. The coupled calculation process is shown in Figure 11.
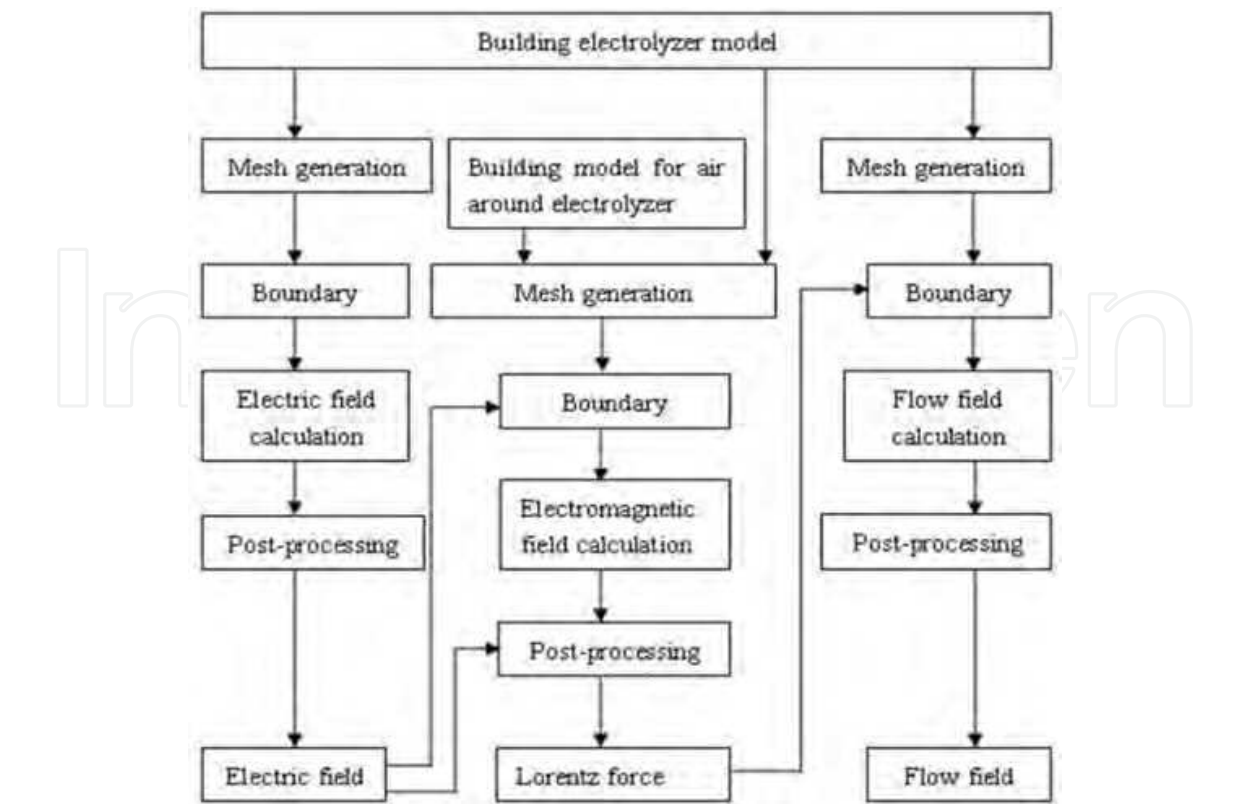
Fig. 11. Calculation procedures for the three-phase flow field under the electromagnetic field

4. Structure of the electrolytic cell and grids for CFD simulation

The advanced diaphragmless magnesium electrolyzer is with the dimension $2.91 \times 1.87 \times 1.40 \text{m}$, eight anodes with dimension $0.95 \times 1.14 \times 0.15 \text{m}$, nine cathodes with dimension $0.95 \times 1.14 \times 0.05 \text{m}$, and the anode and cathode distance as 0.07m. The structure of the electrolytic cell and grids for CFD simulation are shown in Figure 12(a) and Figure 12(b), respectively.

(a)   (b)
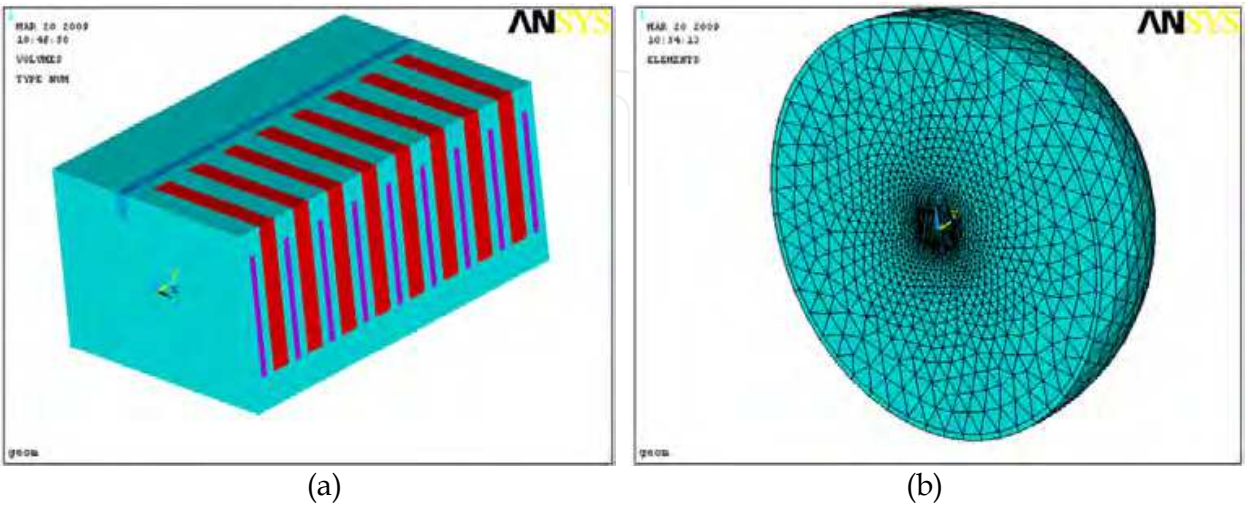
Fig. 12. Structure of the electrolytic cell (a) and grid division for the simulation of the electromagnetic field (b)

During the calculation of the electromagnetic field, the finite element method is employed. According to its symmetry, half of electrolyzer could be used to solve this issue. Therefore, the geometric model for calculation given by Figure 12(a) is the right part of the electrolyzer only, and its mesh partitioning is shown as Figure 12(b). During the calculation of the three-phase flow field, Fluent was employed. The GAMBIT software release 2.2 was used to generate structure and unstructured meshes. The grid in the electrolyzer is showed in Figure 13
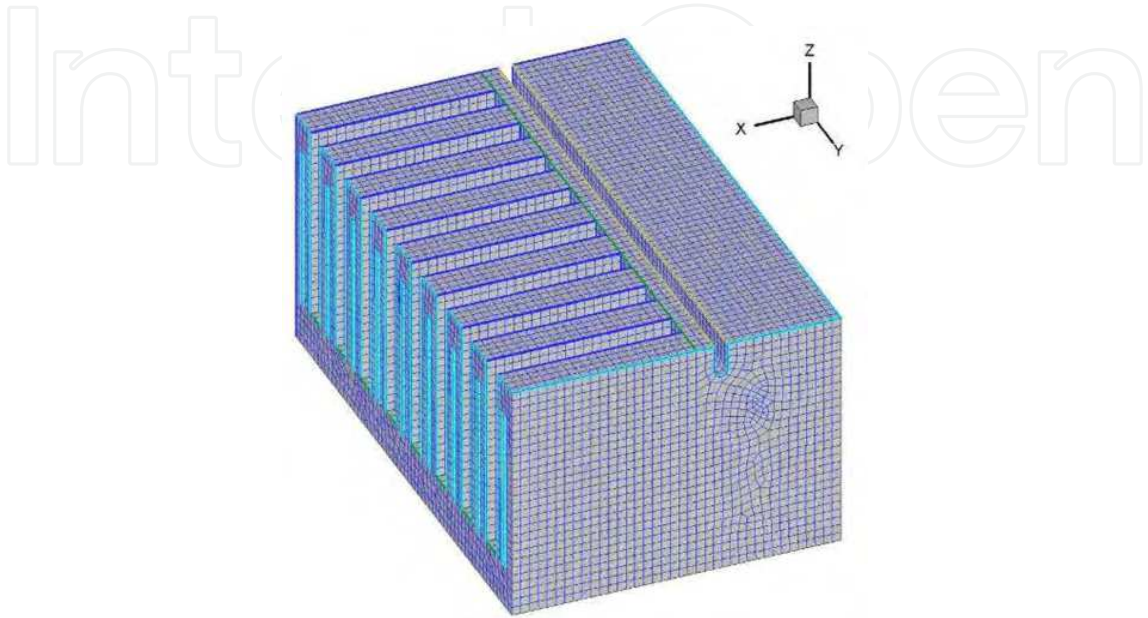
Fig. 13. Grids of the calculation domain for the simulation of the three-phase flow field in electrolyzer

The distribution of the electromagnetic field in the magnesium electrolyzer is calculated using ANSYS 11.0 software, and the properties of materials used for the calculation is shown in table 5. Figure 14 (a) shows the contour of the electric field in the electrolyzer. The voltage energy is concentrated in electrolysis compartment, especially in the space between anode and cathode. From anode to the top of cathode, the value of voltage decreases from maximum to zero. So, in the collection compartment of magnesium, magnesium is not affected by the electric field because of magnesium without charge. This favors the collection of magnesium in collection compartment. Figure 14 (b) shows the contour of voltage on the surface paralleling to work surfaces of electrodes. In the picture, maximum voltage is a constant on the surface of cathode. The value of voltage declines rapidly with distance from the cathode surface.

Material / Properties	Electrolyte	Graghite	Cast steel	Refractory material	Air
Magnetic Permeability	1.0	1.0	1.0	1.0	1.0
Electrical conductivity ($\Omega \cdot m$)	4.0×10^{-3}	8.5×10^{-6}	1.3×10^{-7}	∞	∞

Table 6. Properties of materials used for the calculation of the electromagnetic field

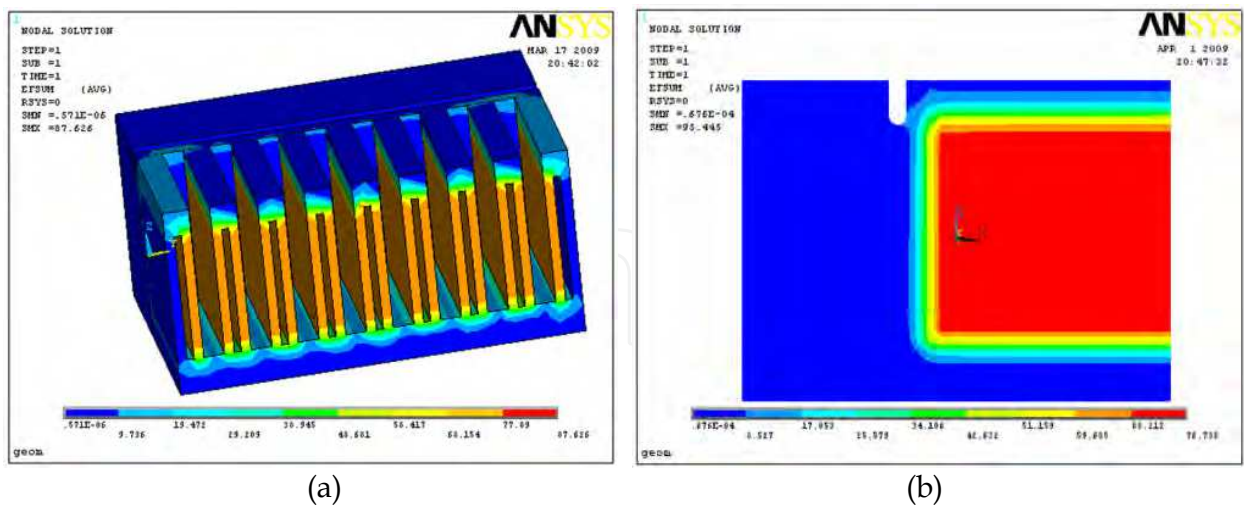(a)   (b)

Fig. 14. Contour of the electric field in the magnesium electrolyzer
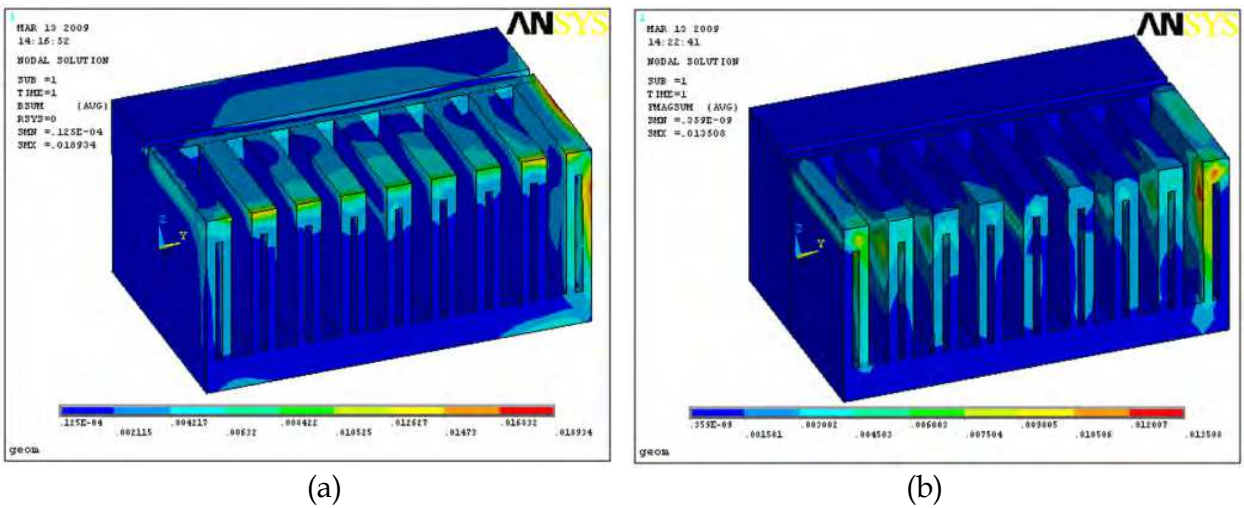

(a)   (b)

Fig. 15. Contours of the electromagnetic field (a) and contours of Lorentz forces(b) in the magnesium electrolyzer

The simulation results in Figure 15 show that the distributions of both the magnetic Field and Lorentz force are vertically symmetrical along the electrolysis compartment, decreasing gradually from the end toward the middle, and the maximum Lorentz force reaching 0.0135N at corner. The typical distribution of Lorentz forces in a plane vertical to work surfaces of electrodes is shown in figure 16 (b). Figure 16(a) shows the relative planes arrangement. As shown in Figure 16, vectors of Lorentz forces pointed to the collection compartment from electrolysis compartment. These directions of Lorentz forces will favor the circulation of electrolyte. Table 6 lists the typical values of Lorentz Forces calculated by ANSYS 11.0 software, these values will be added to the fluid momentum equations (Eq.20) as a source term, in order to couple the effect of the electromagnetic field on the three-phase flow behavior. This is done by using an in-house UDF code during simulations.
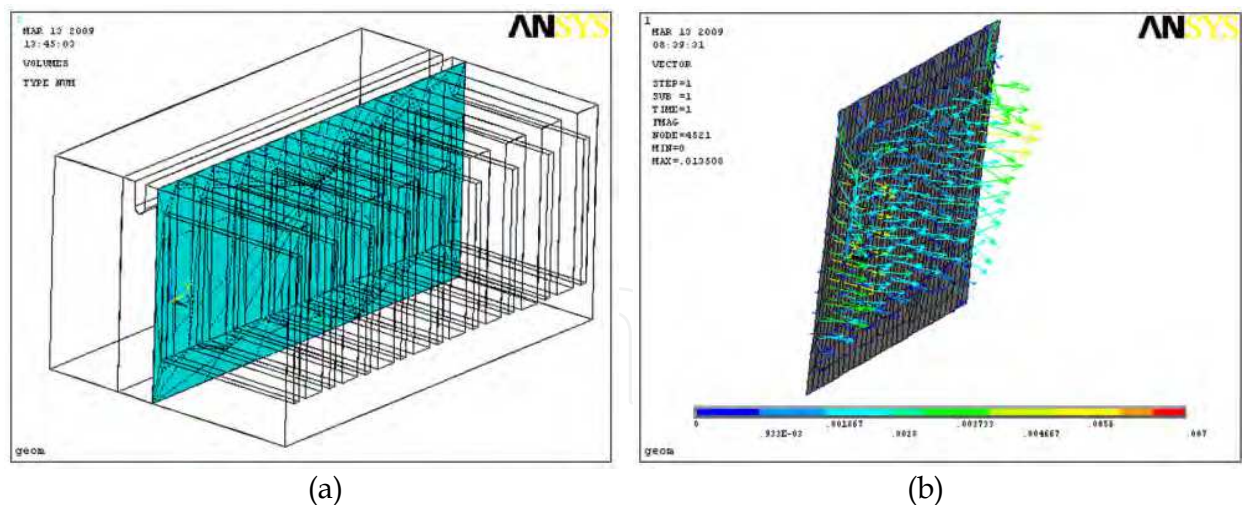
| (a) | (b) |

Fig. 16. Location of plane(b) in the electrolytic cell and Vectors of Lorentz Forces(a)

X /m	Y/m	Z/m	Fx /N	Fy /N	Fz /N
-0.900E-01	0.275E+01	0.934E-01	0.206E-02	0.857E-17	-0.124E-02
-0.400E-01	0.275E+01	0.935E-01	0.167E-02	0.693E-17	-0.111E-02
0.100E-01	0.275E+01	0.936E-01	0.117E-02	0.481E-17	-0.815E-03
…	…	…	…	…	…
-0.302E+00	0.284E+01	0.520E+00	0.262E-05	-0.234E-05	0.437E-06
-0.302E+00	0.289E+01	0.520E+00	0.263E-05	-0.373E-05	0.115E-0.5

Table 7. Distribution of Lorentz force in the electrolyzer

Table 7 lists the properties of fluid used in the simulation of the flow field in the electrolyzer. The typical simulation result is shown in Figure 17. Based on the simulation results, there exist three kinds of circulations in the electrolytic cell, circulation A and D as the same kind near walls, circulation B in the middle of electrolyzer and circulation C is the last one.

Fluid Properties	Electrolyte	chlorine	magnesium
Density(kg/cm^3)	1620	0.9	1500
Viscosity (kg/m·s)	1.68×10^{-3}	2.93×10^{-5}	1.04×10^{-3}

Table 8. Properties of fluids used in the simulation of three-phase flow field

Though analyzing the flow field obtained, we can see that the whole circulation distributes symmetrically along the electrolyzer. Electrolyte in the pair of the cathode and anode does parallel movement between the surfaces of the electrodes such as circulation B. They are the best circulations in the whole electrolyzer, because the circulation had shortest distance from the electrolysis compartment to the collection compartment. Liquid magnesium can be

delivered effectively to the collection compartment by the circulation B of electrolyte. Other circulation between the cathode and anode deflect to the side wall, instead of parallel to the surface of cathode and anode such as circulation C. They are not parallel to the surfaces of electrodes in collection compartment. They are worse than circulation B in the process of production. The worst circulations are circulation A and D, because they are near the wall. The side wall had effects on circulations, so circulation A and D had to run longer distance in electrolyzer. That would decline the efficiency of current. In a word, the structure optimization of the electrolyzer should be designed to ensure electrolyte circulation parallel to the surfaces of electrodes.
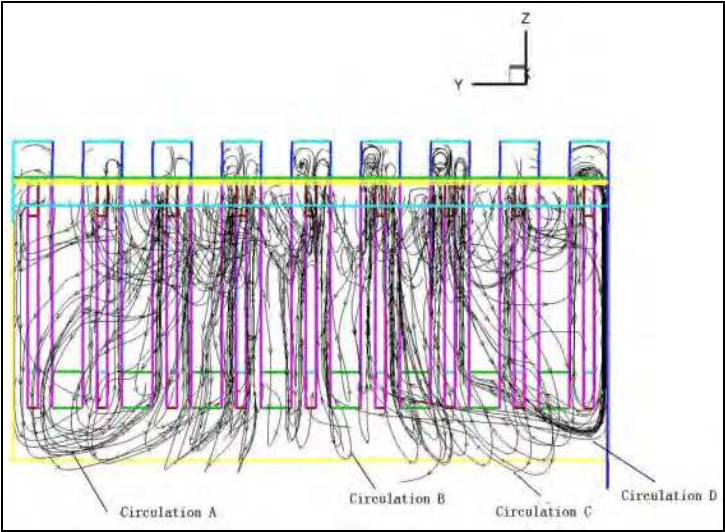
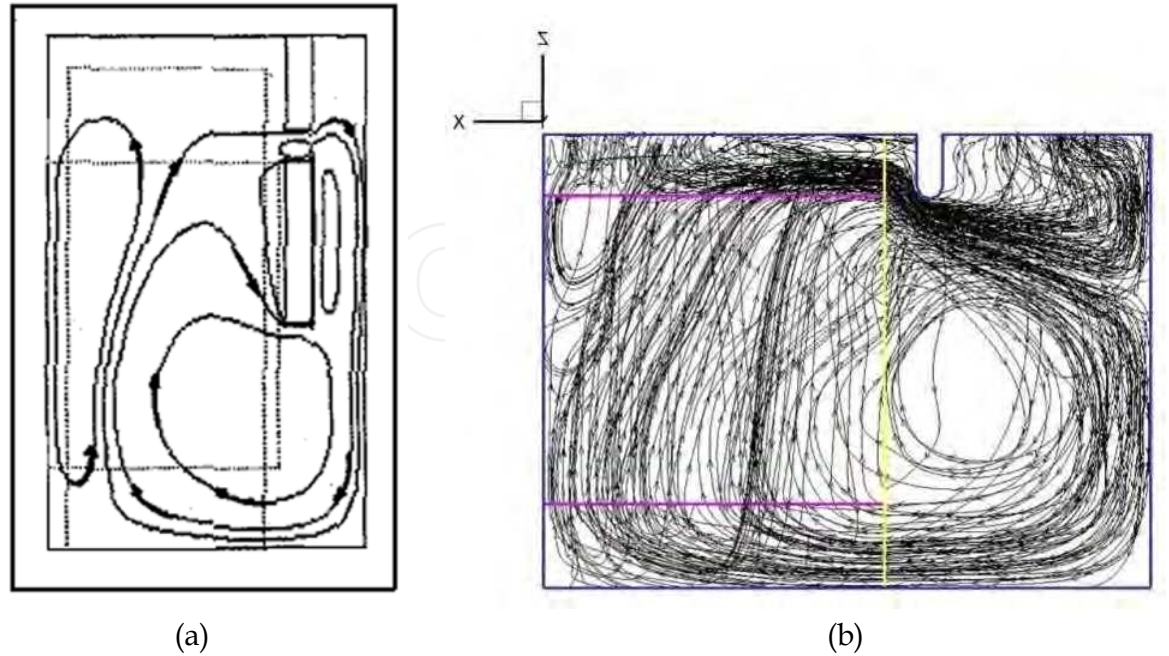Fig. 17. Streamlines of flow field in the electrolyzer at X direction(in front)

(a)   (b)

Fig. 18. Comparisons of the simulation results of the electrolyte circulation between Agalakov's results reported in the literature (a) and our work (b)

In Figure 18, from side view, our simulation result(b) has the main characteristics of flow field in electrolyzer and is similar with Agalakov's result(a) [14]. That is shown our math model is correct. Two main circulations appear as shown in Figure 18, one was big and the other was small. During production, the big one can transport magnesium from the electrolysis compartment to the collection compartment. The small one was near back wall, it will damage the back wall, the phenomena can be tested by an industrial electrolyzer, as shown in Figure 19.

Fig. 19. Damaged back wall of an industrial magnesium electrolyzer due to the frequently washing of the small electrolyte circulation

5. Conclusions

1. After variance analysis, the significance for the recovery rate of silicon oil is in the sequence of θ, ACD and D, and finally W.
2. The largest recycle rate of silicon oil is 91.34 wt-%. After the data processing, the best experimental conditions is 60 mm (ACD), 28 mm (D), 127 mm (W), 12° (θ).
3. In the single parameter experiment, when θ is larger than 12°, φ maintain at the largest level. The deeper of the electrode, the lager recovery rate was. When it reaches 28 mm, the recovery rate tend to be changeless. Near the best experiment conditions, φ tent to be irrelated to ACD.
4. The spray angle for gas from anodic bottom to top maintains at 9°, not change with anodic shape and flow rate.
5. Electric field concentrated in the electrolysis compartment; magnetic Field and Lorentz force distributes vertically symmetrical along the electrolysis compartment, decreasing gradually from the end toward the middle.
6. Electrolyte circulations were divided three different types: parallel to working surfaces of electrodes, not parallel to working surfaces of electrodes and near wall's. The circulations paralleling to working surfaces of electrodes can transport liquid magnesium efficiently from electrochemical compartment to service compartment.
7. The research indicates that the structure optimization of the electrolyzer should be designed to ensure electrolyte circulation parallel to the surfaces of electrodes and removing the adverse effects of the electrolyzer flow field.

6. Acknowledgment

7. References

[1] http://www.roskill.com/reports/magnesium

[2] International Magnesium Association, www.intlmag.org

[3] Friedrich H. E.; Mordike B. L. Magnesium Technology; Springer: Germany, 2006

[4] Emley E.F. Principles of Magnesium Technology; Pergamon: London, 1966

[5] Sivilotti O. G.; Kingston C. Procedures and apparatus for electrolytic production of metals. 1977, US Patent 4055474

[6] Andreassen K. A.; Skien Y. B.; Johnsen H. K.; Ognesal L. B.; Solheim P. R. Method and electrolyzer for production of magnesium. 1981, US Patent 4308116

[7] Holliday R. D.; McIntosh P. Laboratory cell and hydrodynamic model studies of magnesium chloride reduction in low-density electrolytes. *J. Electrochem. Soc.* 1973, 120, 858

[8] Burnakin V. V.; Shestakov V. M.; Sorokous V. G.; Borutto G. M. Hydrodynamics of flow in the interelectrode space of magnesium electrolyzers. *Tsvetn. Metall.* 1989, (4), 62

[9] Burnakin, V. V.; Polyakov, P. V.; Shestakov, V. M. Kolesnikov V. A. Analytical calculation of characteristics of two-phase flows in magnesium electrolytic cells. *Tsvetn. Met.* 1979, (8), 73

[10] Korobov M. A. Mathematical model of a magnesium electrolytic cell. *Tsvetn. Met.* 1983, (5), 53

[11] Scherbinin S. A.; Yakovleva G. A.; Fazylov A. F. Mathematical model of thermal and electric fields in a magnesium electrolytic cell. *Tsvetn. Met.* 1994, (4), 60

[12] Shcherbinin S. A.; Yakovleva G. A.; Kazylov A. K. Numerical study of thermal and electric fields of a magnesium electrolytic cell. *Tsvetn. Met.* 1994, (6), 68

[13] Shcherbinin S. A.; Fazylov A. R.; Yakovleva G. A. Mathematical simulation of three-dimensional thermal and electric fields of magnesium electrolyzer. *Tsvetn. Met.* 1997, (5), 79

[14] Agalakov V. V.; Shcherbinin S. A.; Yakovleva G. A. Mathematical simulation of gas-hydrodynamic processes in a magnesium electrolyzer. *Tsvetn. Met.* 1997, (7), 74

[15] Sun Z.; Zhang H. N.; Li P.; Li B.; Lu G. M.; Yu J. G. Modeling and simulation of the flow field in the electrolysis of magnesium". *JOM.* 2009, 61, 29

[16] Gökhan D.; Karakaya İ. Electrolytic magnesium production and its hydrodynamics by using an Mg–Pb alloy cathode. *J. Alloy. Compd.* 2008, 465, 255

[17] Dernedde E.; Cambridge E.L. Gas induced circulation in an aluminum reduction cell. *light met.* 1975, 111.

[18] Sun Z.; Zhang H. N.; Li B.; Lu G. M.; Yu J. G. Effect of Electromagnetic Field on Three-Phase Flow Behavior. Ind. Eng. Chem. Res. 2010, 49, 10798

[19] Zhang Y. H.; Yang C.; Mao Z. S. Large eddy simulation of the gas-liquid flow in sstirred tank. AIChE J. 2008, 54, 1963

[20] Jain M.; Paranandi M.; Roush D.; Göklen K.; Kelly W. J. Using CFD to understand how flow patterns affect retention of cell-sized particles in a tubular bowl centrifuge. *Ind. Eng. Chem. Res.* 2005, 44, 7876

[21] Panneerselvam R.; Savithri S.; Surender G. D. CFD simulation of hydrodynamics of gas-liquid-solid fluidised bed reactor. *Chem. Eng. Sci.* 2009, 64, 1119
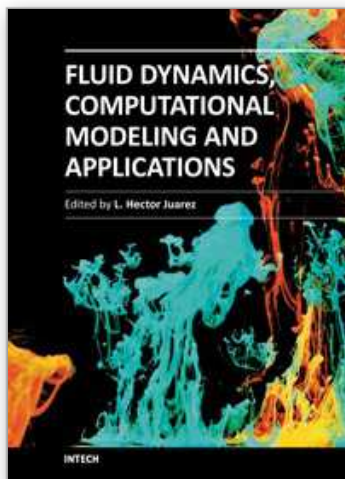
Fluid Dynamics, Computational Modeling and Applications

Edited by Dr. L. Hector Juarez

ISBN 978-953-51-0052-2

Hard cover, 660 pages

Publisher InTech

Published online 24, February, 2012

Published in print edition February, 2012

The content of this book covers several up-to-date topics in fluid dynamics, computational modeling and its applications, and it is intended to serve as a general reference for scientists, engineers, and graduate students. The book is comprised of 30 chapters divided into 5 parts, which include: winds, building and risk prevention; multiphase flow, structures and gases; heat transfer, combustion and energy; medical and biomechanical applications; and other important themes. This book also provides a comprehensive overview of computational fluid dynamics and applications, without excluding experimental and theoretical aspects.

How to reference

In order to correctly reference this scholarly work, feel free to copy and paste the following:

Ze Sun, Guimin Lu, Xingfu Song, Shuying Sun, Yuzhu Sun, Jin Wang and Jianguo Yu (2012). Study on Multi-Phase Flow Field in Electrolysis Magnesium Industry, Fluid Dynamics, Computational Modeling and Applications, Dr. L. Hector Juarez (Ed.), ISBN: 978-953-51-0052-2, InTech, Available from: http://www.intechopen.com/books/fluid-dynamics-computational-modeling-and-applications/study-on-multi-phase-flow-field-in-electrolysis-magnesium-industry

INTECH
open science | open minds